Supporting Information

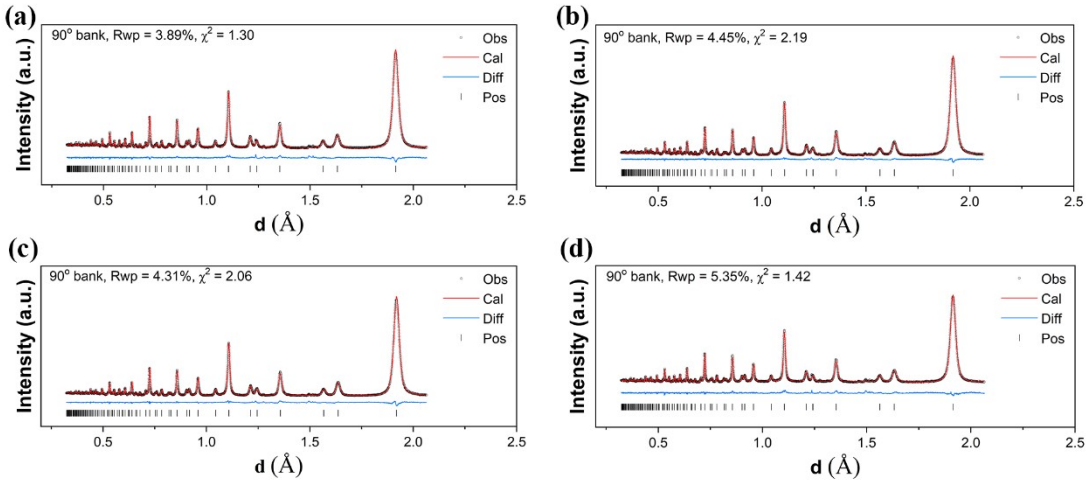

Figure S1. Rietveld refining of (a) as-prepared CeO_2; (b) CeO_2 reduced at 400 °C (without the consideration of H species); (c) CeO_2 reduced at 400 °C (with the consideration of H species); (d) Oxidized CeO_2. The different curves (blue curves) of these four patterns are basically straight lines, and the value of Rwp and χ^2 are very small, which represent the high rationality of these refinement results.

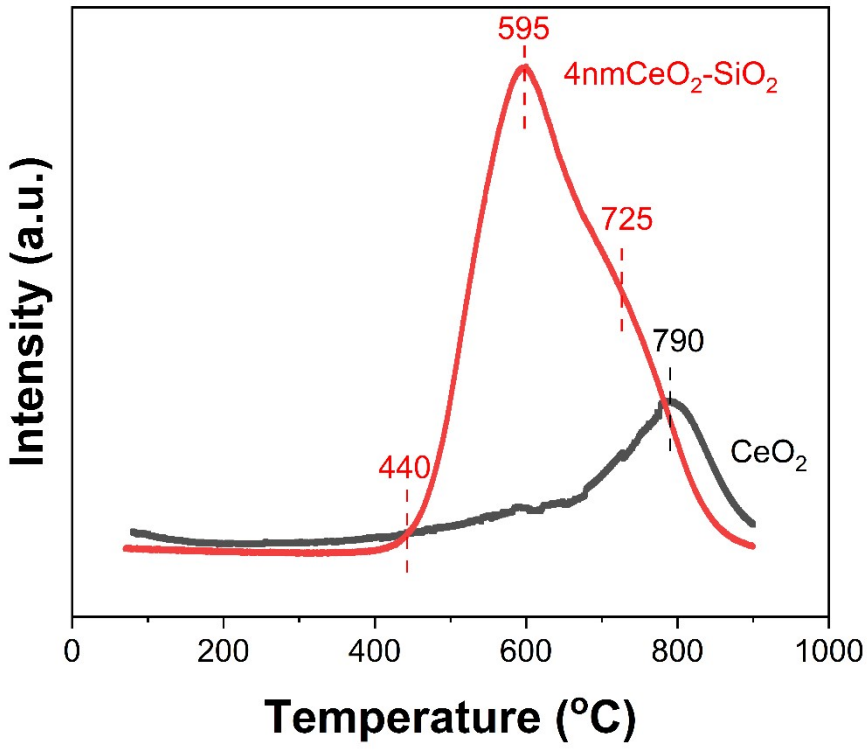

Figure S2. TPD of CeO_2 and 4nmCeO_2-SiO_2 that were pre-reduced at 400 °C. The signal of m/z=2 was recorded and display in this picture. Experiment condition: heating rate 5 °C/min, vented with 30 mL/min Ar.

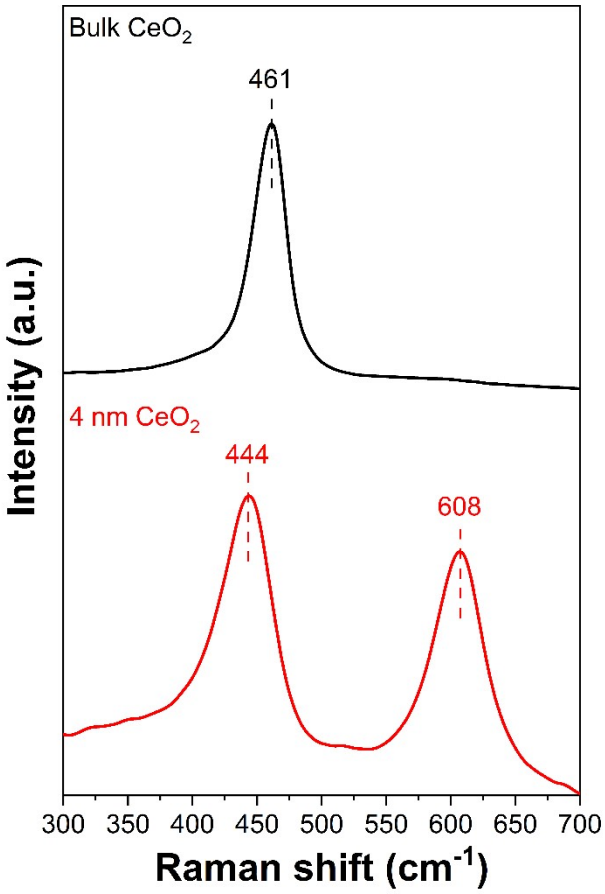

Figure S3. Raman spectra of bulk CeO_2 and 4 nm CeO_2.

Supplementary discussion for **Figure S3**:

Raman spectrum is a common characterization for oxygen vacancy in CeO_2.[1, 2] There is only one Raman peak located at 461 cm^{-1} in bulk CeO_2, which is the F_{2g} symmetric breathing mode of lattice O atoms. Once CeO_2 nanoparticle size is decreased to ~4 nm, a new Raman peak located at 608 cm^{-1} was observed. This peak is attributed to oxygen vacancy in CeO_2 lattice.[3, 4] This comparison indicates that decreasing CeO_2 nanoparticle size to ~4 nm could greatly improve the oxygen vacancy concentration compared to bulk CeO_2.

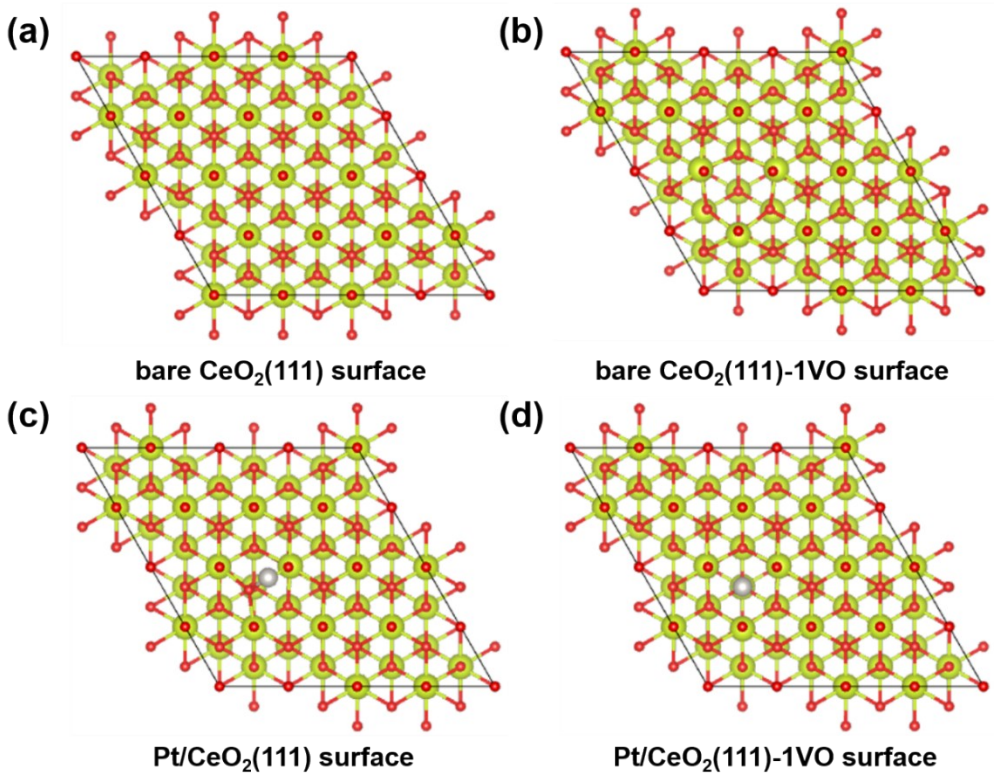

Figure S4. The models of (a) bare CeO_2(111) surface, (b) bare CeO_2(111) surface with 1 oxygen vacancy (VO), (c) Pt deposited on CeO_2(111) surface and (d) Pt deposited on CeO_2(111) surface with 1 VO. Yellow: Ce atom, red: O atom, gray: Pt atom.

Supplementary discussion for **Figure S4**:

The CeO_2 support in **Figure S4**(a,c) is composed of 96 O atoms and 48 Ce atoms by forming three layers. In comparison, defected CeO_2 support in **Figure S4**(b,d) is composed of 95 O atoms and 48 Ce atoms by removing one O atom on the first layer of CeO_2 support. Pt atom is placed on the location of oxygen vacancy on defected CeO_2 support. In comparison, Pt atom is also placed on similar location of CeO_2 support. The single point energies of **Figure S4** are listed in **Table S1**.

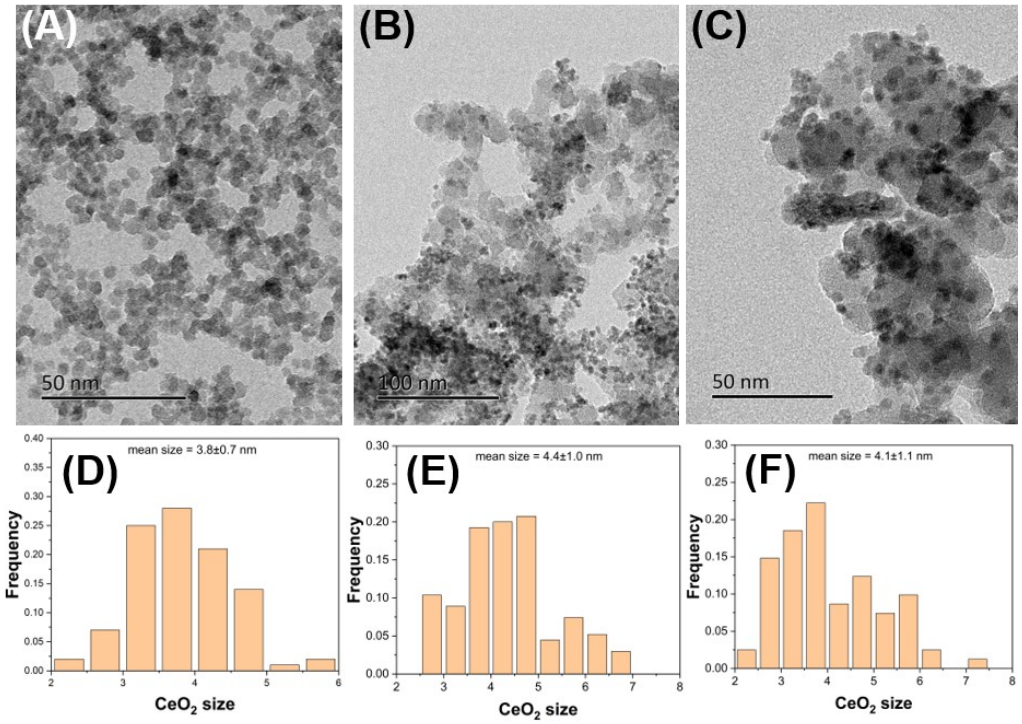

Figure S5. TEM image of (A) 4 nm CeO_2 colloid, (B) 4nmCeO_2-SiO_2 and (C) 4nmCeO_2-SiO_2 after 400 °C reduction for 2 h. CeO_2 nanoparticle size distribution of (D) 4 nm CeO_2 colloid, (E) 4nmCeO_2-SiO_2 and (F) 4nmCeO_2-SiO_2 after 400 °C reduction for 2 h.

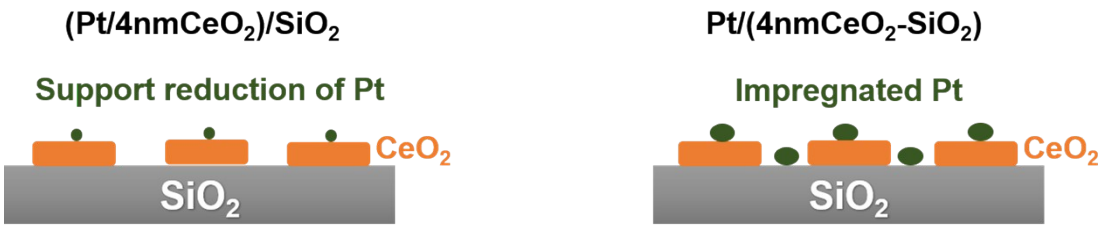

Figure S6. Catalyst models of (Pt/4nmCeO_2)/SiO_2 and Pt/(4nmCeO_2-SiO_2).

Supplementary discussion for **Figure S6**:

During the preparation of (Pt/4nmCeO_2)/SiO_2 sample via SRS, the reductive centers on 4 nm CeO_2 nano-islands react with the H_2PtCl_6 precursor, leading to the Pt deposition on CeO_2 surface. In contrast, the pre-reduction generates no reducing species on SiO_2 surface due to its irreducible property. The lack of chemical reactions between SiO_2 surface and H_2PtCl_6 precursor leads to the weak interaction between Pt and SiO_2. Furthermore, the deionized water washing at the last step of catalyst preparation could remove Pt atoms that are weakly bound on 4nmCeO_2/SiO_2 surface.

On the other hand, Pt/(4nmCeO_2-SiO_2) is prepared by impregnation method, which could not control the location of Pt. Thus, the Pt was randomly deposited on 4nmCeO_2-SiO_2 support. There is only 10wt% 4 nm CeO_2 nano-islands in 4nmCeO_2-SiO_2 support, so the SiO_2 surface is the dominate surface in this support. Therefore, once Pt is randomly deposited on 4nmCeO_2-SiO_2 support with impregnation, most Pt species are located on SiO_2 surface.

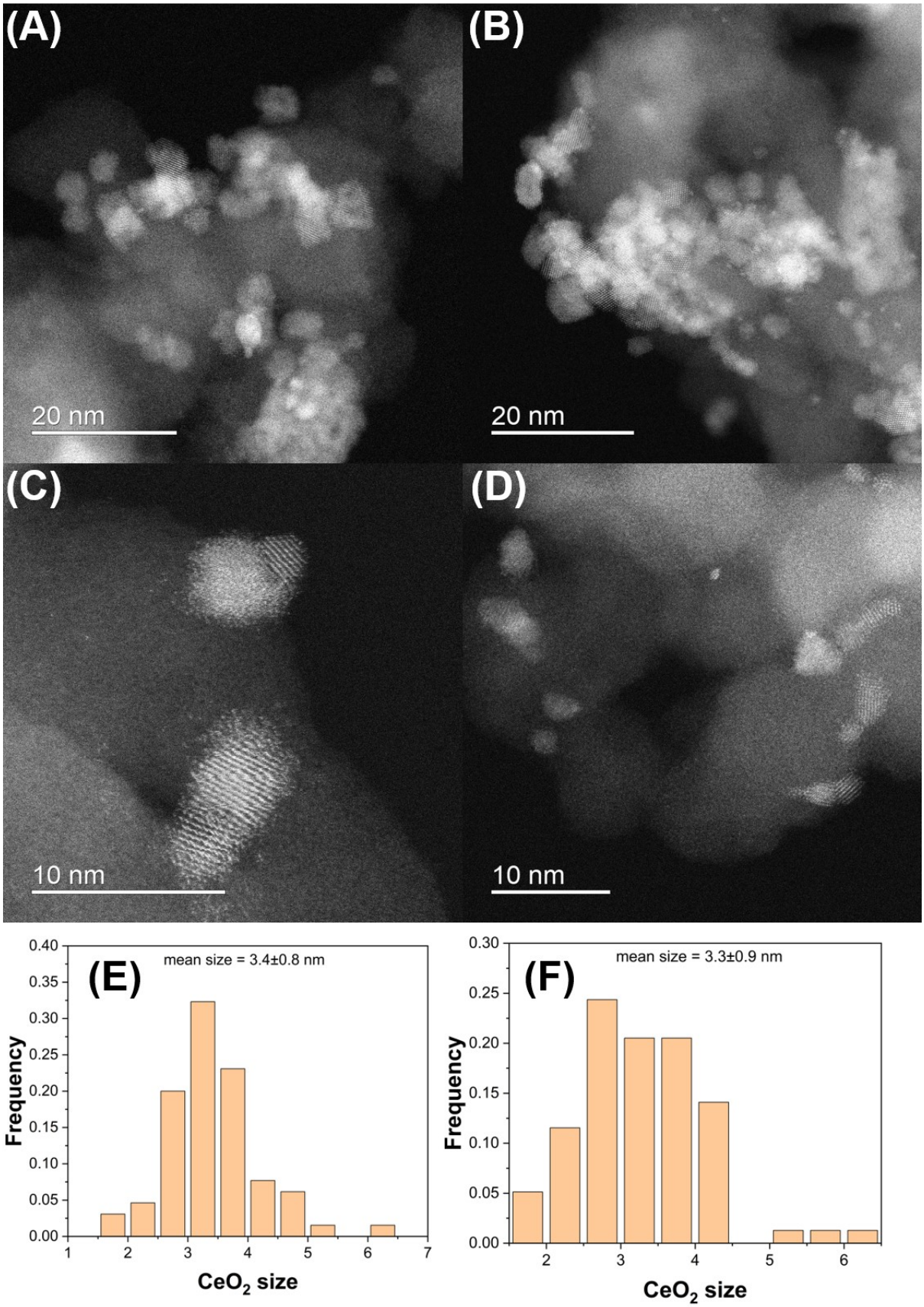

Figure S7. HADDF-STEM images of (A,C) (Pt/4nmCeO_2)/SiO_2 and (B,D) Pt/(4nmCeO_2-SiO_2) with various scale bars. CeO_2 nanoparticle size distribution in (E) (Pt/4nmCeO_2)/SiO_2 and (F) Pt/(4nmCeO_2-SiO_2).

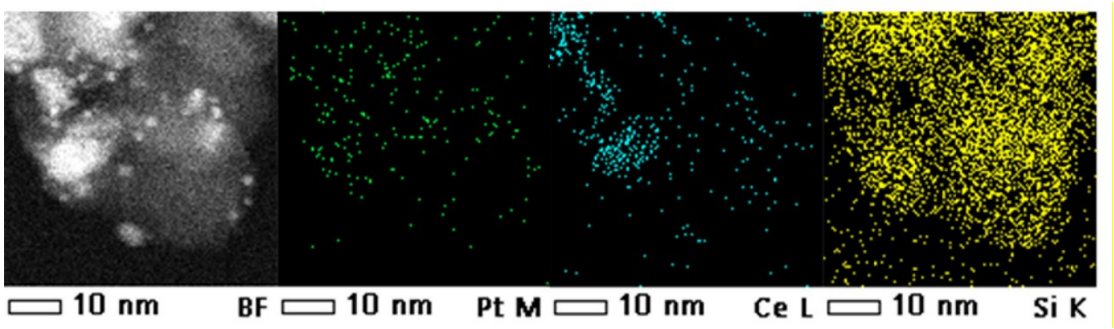

Figure S8. Energy dispersive spectrometer (EDS) mapping of (Pt/4nmCeO_2)/SiO_2.

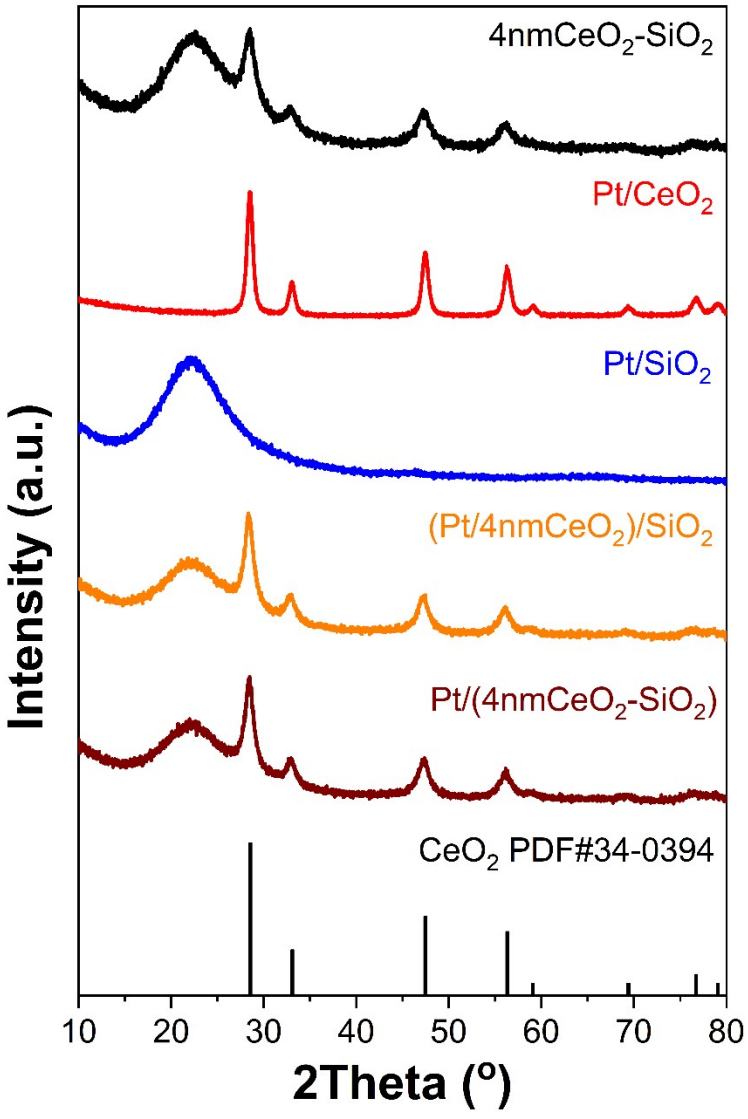

Figure S9. XRD patterns of (Pt/4nmCeO_2)/SiO_2, Pt/(4nmCeO_2-SiO_2), and control catalysts.

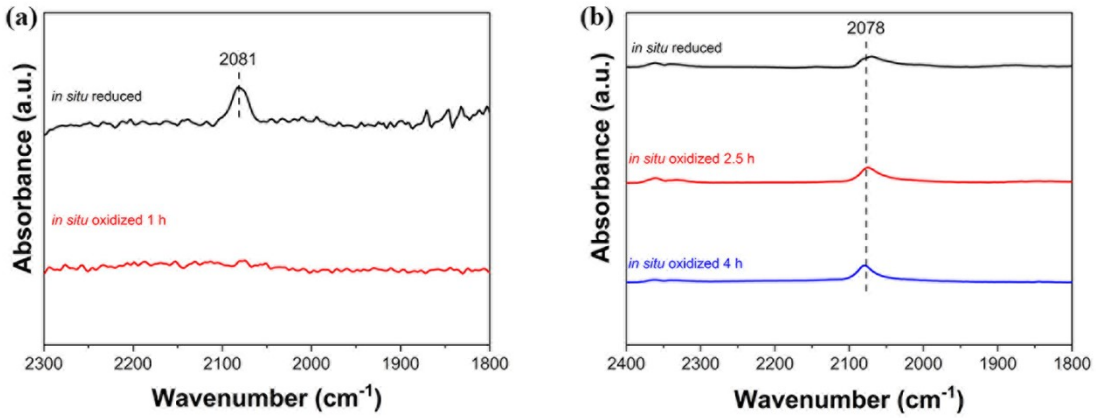

Figure S10. CO-FTIR spectra of (a) Pt/CeO_2, (b) Pt/SiO_2.

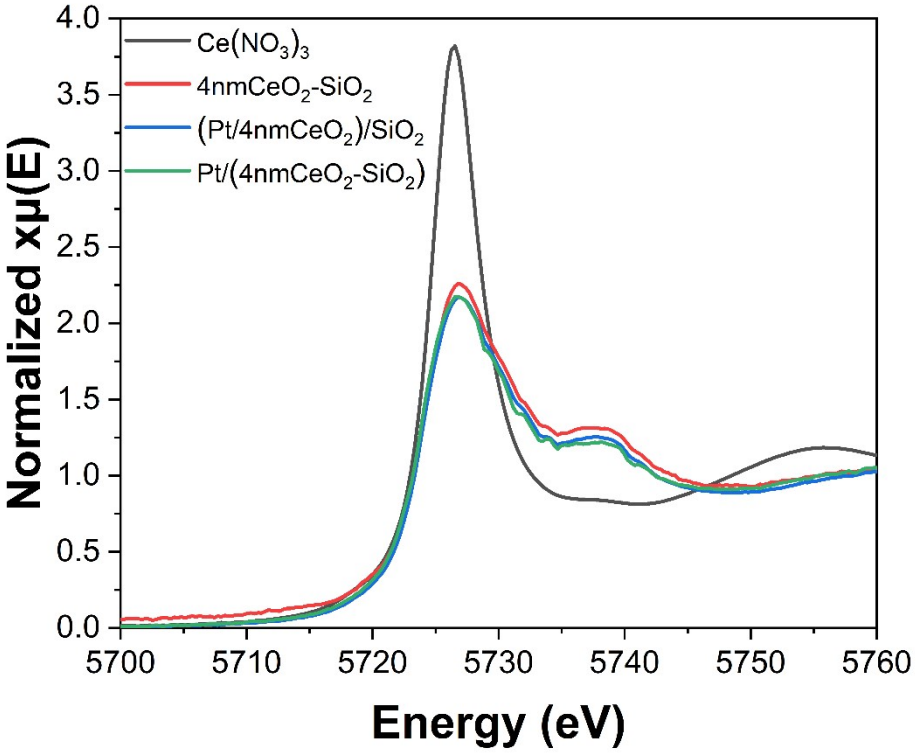

Figure S11. XANES of Ce L_3 edge of *in situ* reduced $4nmCeO_2$-SiO_2, $(Pt/4nmCeO_2)/SiO_2$ and $Pt/(4nmCeO_2$-$SiO_2)$. $Ce(NO_3)_3$ is set as a reference sample.

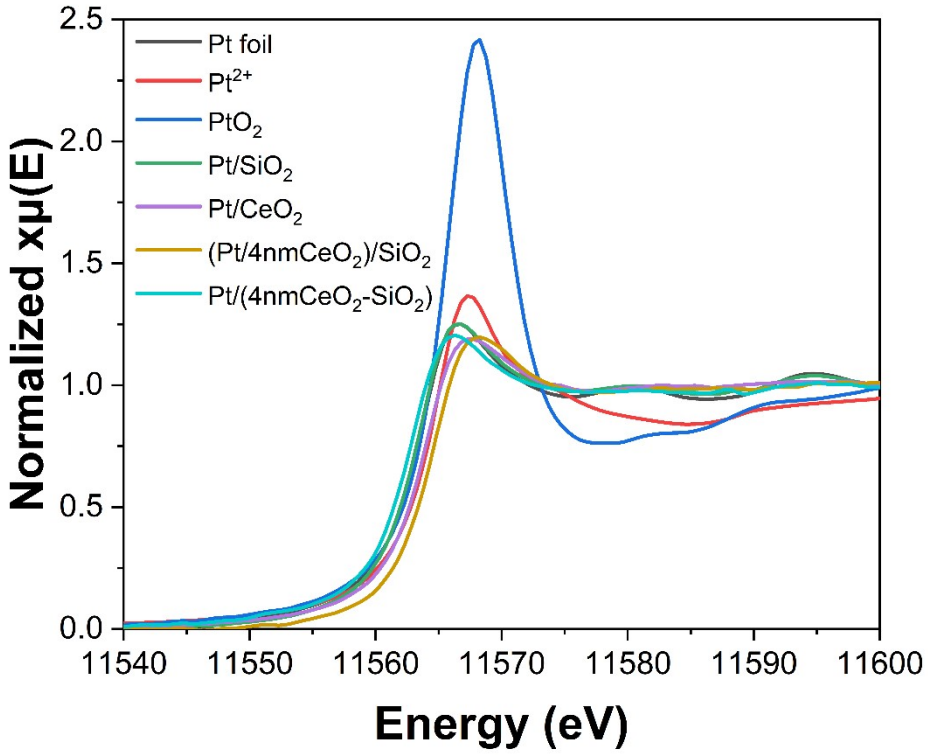

Figure S12. XANES of Pt L_3 edge of *in situ* reduced Pt/SiO_2, Pt/CeO_2, $(Pt/4nmCeO_2)/SiO_2$ and $Pt/(4nmCeO_2\text{-}SiO_2)$. PtO_2 was used as a reference standard for Pt^{4+}. $Pt(NH_3)_4(NO_3)_2$ was used as a reference standard for Pt^{2+}. Pt foil was used as a reference standard for Pt^0.

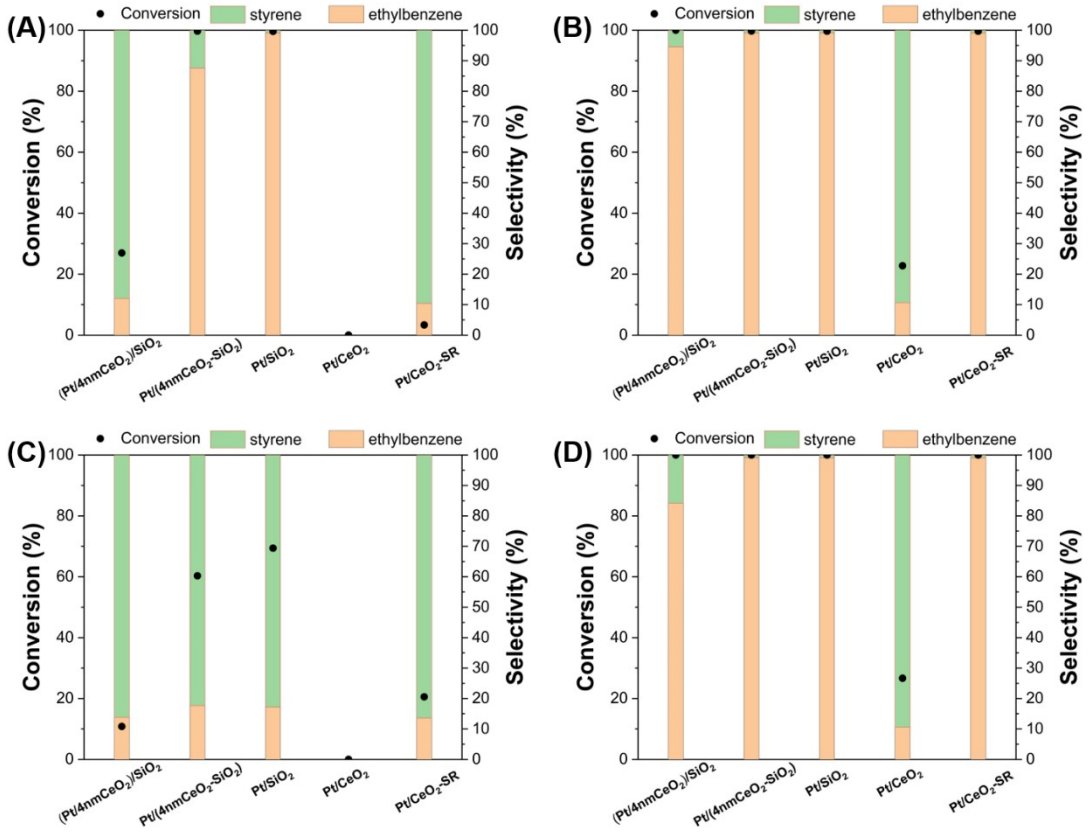

Figure S13. Phenylacetylene hydrogenation under (A) 0.5 MPa H_2, 1h; (B) 2 MPa H_2, 1 h; (C) 1 MPa H_2, 0.5 h and (D) 1 MPa H_2, 2 h. Additional conditions: 0.4 mmol phenylacetylene, 40 °C. Circles: conversion. Bars: selectivity of styrene and ethylbenzene.

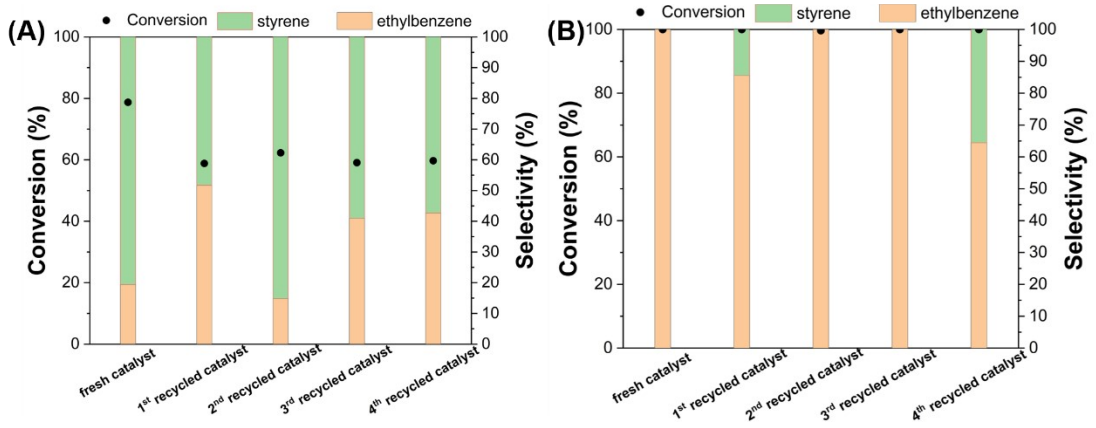

Figure S14. Catalyst recycle test of (A) (Pt/4nmCeO_2)/SiO_2; (B) Pt/(4nmCeO_2-SiO_2). Conditions: 0.4 mmol phenylacetylene, 1 MPa H_2, 1 h, 40 °C. Circles: conversion. Bars: selectivity of styrene and ethylbenzene.

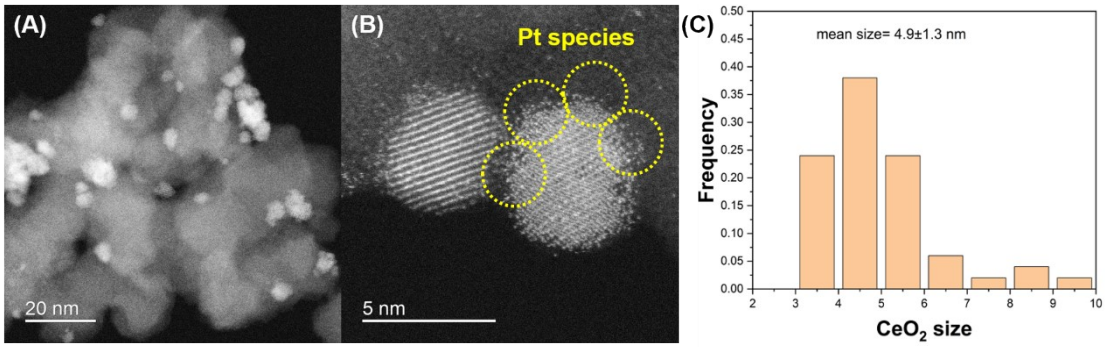

Figure S15. HADDF-STEM images of 4th recycled (Pt/4nmCeO_2)/SiO_2 catalyst.

Table S1. The Pt binding energy on CeO_2(111) surface.

Models	1 VO on CeO_2(111)	Perfect CeO_2(111)
CeO_2(111) (eV)	-1159.6300	-1168.3951
Pt single atom (eV)	2.3733	2.3733
Pt/CeO_2 (eV)	-1161.3518	-1168.1295
Pt binding energy (eV)	-4.0951	-2.1077

Supplementary description for **Table S1**:

Table S1 summarizes the single point energy of different models displayed in **Figure S4**, upon which the Pt binding energy is calculated. For example, the single point energy of CeO_2(111) surface (96 O atoms + 48 Ce atoms) is -1168.3951 eV according to the OUTCAR file of VASP. And the single point energy of Pt single atom is 2.3733 eV. Once Pt is placed on the CeO_2(111) surface, its overall single point energy becomes -1168.1295 eV. Therefore, the Pt binding energy on perfect CeO_2(111) surface is calculated as -2.1077 eV. On the other hand, the Pt binding energy in the oxygen vacancy of CeO_2(111) surface is calculated as -4.0951 eV. Based on these two binding energies, it is concluded that Pt has stronger interaction with defected CeO_2 surface.

Table S2. ICP-OES characterization for Pt on different samples.

Samples	Pt loading amount/wt%
Pt/CeO_2-SR	0.37
Pt/CeO_2-NR	0.14
$(Pt/4nmCeO_2)/SiO_2$	0.23
$(Pt/4nmCeO_2)/SiO_2$-NR	0.08

Supplementary description for **Table S2**:

The key difference between Pt/CeO_2-SR and Pt/CeO_2-NR, $(Pt/4nmCeO_2)/SiO_2$ and $(Pt/4nmCeO_2)/SiO_2$-NR is whether there is a pre-reduction step. It is expected that if reducing species (adsorbed H species and Ce^{3+} species) are fully oxidized as soon as CeO_2 and $4nmCeO_2/SiO_2$ are taken out from reducing furnace, the Pt loading amount on all four samples should be similar because the feeding amount ratios of Pt : CeO_2 and Pt : ($4nmCeO_2$-SiO_2) were controlled as 0.5wt% in all preparations. **Table S2** shows the Pt loading amount of these four samples, and it is observed that the pre-reduction treatment improves Pt loading amount on both CeO_2 support and $4nmCeO_2/SiO_2$ support. This observation proves that not all reducing species (adsorbed H species and Ce^{3+} species) generated in pre-reduction is oxidized once the bare supports (bulk CeO_2 and $4nmCeO_2$-SiO_2) are exposed to air at room temperature.

Table S3. XANES spectra of Ce L_3 edge of *in situ* reduced $4nmCeO_2$-SiO_2, $(Pt/4nmCeO_2)/SiO_2$ and $Pt/(4nmCeO_2$-$SiO_2)$.[1]

Sample	Ce^{3+}/wt%	Ce^{4+}/wt%	R-factor
$4nmCeO_2$-SiO_2	49.9	50.1	0.016
$(Pt/4nmCeO_2)/SiO_2$	49.4	50.6	0.019
$Pt/(4nmCeO_2$-$SiO_2)$	51.8	48.2	0.027

[1]For the LCF, CeO_2 was used as a reference standard for Ce^{4+}; $Ce(NO_3)_3{\cdot}6H_2O$ was used as a reference standard for Ce^{3+}. CeO_2:SiO_2=1:10 (w/w) in all samples. $(Pt/CeO_2)/SiO_2$ and $Pt/(CeO_2$-$SiO_2)$ are *in situ* reduced.

Table S4. XANES spectra of Pt L_3 edge of *in situ* reduced Pt/SiO_2, Pt/CeO_2, $(Pt/4nmCeO_2)/SiO_2$ and $Pt/(4nmCeO_2$-$SiO_2)$ samples.[1]

Sample	Pt^0/wt%	Pt^{2+}/wt%	Pt^{4+}/wt%	R-factor
Pt/SiO_2	100	0	0	0.038
Pt/CeO_2	81.0	0	19.0	0.006
$(Pt/4nmCeO_2)/SiO_2$	47.4	0	52.6	0.037
$Pt/(4nmCeO_2$-$SiO_2)$	100	0	0	0.011

[1]For the LCF, PtO_2 was used as a reference standard for Pt^{4+}. $Pt(NH_3)_4(NO_3)_2$ was used as a reference standard for Pt^{2+}. Pt foil was used as a reference standard for Pt^0.

Table S5. Pt loading amount during catalyst stability test characterized by ICP-OES.

Pt loading amount/wt%	$(Pt/4nmCeO_2)/SiO_2$	$Pt/(4nmCeO_2$-$SiO_2)$
Fresh catalyst	0.2376	0.1977
1st recycled catalyst	0.1843	0.1277
2nd recycled catalyst	0.1677	0.1059
3rd recycled catalyst	0.1544	0.1094
4th recycled catalyst	0.1335	0.1063

Table S6. CeO_2 loading amount during catalyst stability test characterized by ICP-OES.

CeO_2 loading amount/wt%	$(Pt/4nmCeO_2)/SiO_2$	$Pt/(4nmCeO_2$-$SiO_2)$
Fresh catalyst	6.5790	7.8509
1st recycled catalyst	6.7438	5.0041
2nd recycled catalyst	6.8105	4.3174
3rd recycled catalyst	7.1054	5.8882
4th recycled catalyst	6.1070	4.7866

Table S7. Phenylacetylene hydrogenation reported in other references.

Catalyst	Temperature/°C	Conversion/%	Selectivity/%	Reference
Au/graphene oxide	60	99	99	5
PdZn@ZIF-8	100	95	92	6

Pt colloid	50	99	90.2	7
Pd/Al_2O_3	50	99	96	8

References

1. Z. Zhang; Y. Wang; J. Lu; J. Zhang; M. Li; X. Liu; F. Wang, *ACS Catalysis* **2018,** *8*, 2635.
2. Z. Zhang; Y. Wang; J. Lu; C. Zhang; M. Wang; M. Li; X. Liu; F. Wang, *ACS Catalysis* **2016,** *6*, 8248.
3. M. Guo; J. Lu; Y. Wu; Y. Wang; M. Luo, *Langmuir* **2011,** *27*, 3872.
4. Z. Wu; M. Li; J. Howe; H. M. Meyer, III; S. H. Overbury, *Langmuir* **2010,** *26*, 16595.
5. L. Shao; X. Huang; D. Teschner; W. Zhang, *ACS Catalysis* **2014,** *4*, 2369.
6. P. Weerachawanasak; O. Mekasuwandumrong; M. Arai; S.-I. Fujita; P. Praserthdam; J. Panpranot, *Journal of Catalysis* **2009,** *262*, 199.
7. S. Domínguez-Domínguez; Á. Berenguer-Murcia; D. Cazorla-Amorós; Á. Linares-Solano, *Journal of Catalysis* **2006,** *243*, 74.
8. S. Domínguez-Domínguez; Á. Berenguer-Murcia; Á. Linares-Solano; D. Cazorla-Amorós, *Journal of Catalysis* **2008,** *257*, 87.